


UOCS

X. Rich collection of post-mass-transfer systems in NGC 6791[★]

Vikrant V. Jadhav^{1,2} , Annapurni Subramaniam³, and Ram Sagar³

¹ Helmholtz-Institut für Strahlen- und Kernphysik, Universität Bonn, Nussallee 14-16, 53115 Bonn, Germany
e-mail: vjadhav@astro.uni-bonn.de

² Inter-University Centre for Astronomy and Astrophysics (IUCAA), Post Bag 4, Ganeshkhind, Pune 411007, India

³ Indian Institute of Astrophysics, Koramangala II Block, Bangalore 560034, India
e-mail: purni@iiap.res.in; ramsagar@iiap.res.in

Received 13 January 2023 / Accepted 27 June 2023

ABSTRACT

Aims. NGC 6791 is one of the richest old open clusters in the Milky Way. Its position above the Galactic plane and its number density make it an interesting middle ground between Galactic open and globular clusters. We aim to detect the UV-bright population of NGC 6791 using AstroSat/UVIT images in near-UV and far-UV filters and characterise the known post-mass-transfer systems such as blue straggler stars (BSSs).

Methods. We identified 20 members with large UV flux (out of 91 cluster members among 1180 detections) – which is suggestive of binarity, interactions, or stellar activity – using a multi-wavelength spectral energy distribution analysis.

Results. We characterised 62 isolated cluster members, including five hot subdwarfs (sdA/sdB). Additionally, we detected ten sdA/sdB/extremely low-mass (ELM) white dwarf-type candidates hidden alongside other cluster members. Additionally, we report the discovery of four candidate blue lurkers, which are main sequence stars with mass accretion history.

Conclusions. We report that this cluster has a variety of stellar (pre-)remnants, such as sdBs, sdAs, and ELM white dwarfs, which are by-products of binary evolution. These are likely to be post-mass-transfer binaries found throughout the evolutionary phases from the main sequence to the post-horizontal branch. Therefore, this dynamically old open cluster is unique, making it an ideal test bed for dynamical studies.

Key words. binaries: general – open clusters and associations: individual: NGC 6791 – ultraviolet: stars – catalogs

1. Introduction

Open clusters are integral to studies of stellar populations because of their relative homogeneity (in metallicity and age) and robust cluster membership thanks to precise astrometry. Ultraviolet imaging has proven very useful in identifying optically subluminal stars, such as white dwarfs (WDs) and hot subdwarfs (Sahu et al. 2019; Jadhav et al. 2021; Rao et al. 2022). We are currently conducting an Ultraviolet Imaging Telescope (UVIT) based UVIT Open Cluster Study (UOCS) to understand the UV-bright population, focusing on post-mass-transfer systems. M 67 has been found to be home to multiple extremely low-mass (ELM) WDs, which are products of mass transfer (Sindhu et al. 2019; Jadhav et al. 2019; Subramaniam et al. 2020; Pandey et al. 2021; Vernekar et al. 2023). Similar mass-transfer binaries have been found in NGC 7789 (Vaidya et al. 2022) and NGC 2506 (Panthi et al. 2022). Here, we extend this study to the open cluster NGC 6791 ($\alpha_{2000} = 19^{\text{h}}20^{\text{m}}53^{\text{s}}$; $\delta_{2000} = +37^{\circ}46'18''$; $l = 69^{\circ}959$; $b = +10^{\circ}904$), which is ~ 8.5 Gyr old and also one of the metal-rich clusters ($[\text{Fe}/\text{H}] \sim 0.4$) known in the Milky Way (Bossini et al. 2019). It is located at a distance of ~ 4.1 Kpc and is a well-studied massive ($\sim 5000 M_{\odot}$) open star cluster.

Using ground-based and *Kepler* photometry and multi-epoch spectroscopy data, Brogaard et al. (2018) identified the binary star V106 as a blue straggler star (BSS) member of NGC 6791. These authors derived the primary mass as $1.67 M_{\odot}$, which is more massive than the cluster turn-off mass, and the secondary star as a bloated (proto) ELM helium WD. A detailed study also reveals that V106 is potentially a prototype progenitor of an old field giant masquerading as a young one. Villanova et al. (2018) presented and discussed detailed abundances of 17 evolved stars of NGC 6791 using high-resolution spectra obtained with the Ultraviolet and Visible Echelle Spectrograph at the European Southern Observatory Very Large Telescope and High Resolution Echelle Spectrometer at the Keck telescope. These authors obtained a mean $[\text{Fe}/\text{H}] = +0.313 \pm 0.005$, in good agreement with recent estimates. Tofflemire et al. (2014) provided the epoch radial velocity (RV) and related results for 280 stars, including main sequence (MS), red giant branch (RGB), and horizontal branch (HB) stars. Jadhav & Subramaniam (2021) identified 47 potential BSSs in NGC 6791 using *Gaia* DR2 data. Kamann et al. (2019) combined *Gaia* data with the archival line-of-sight velocities and studied the internal dynamics of the NGC 6791 in three dimensions. Martinez-Medina et al. (2018) performed an orbital analysis within a Galactic model (including spiral arms and a bar) and found that it is plausible that NGC 6791 formed in the inner thin disc or the bulge and was later displaced by radial migration to its current orbit. The birth-place and journey of NGC 6791 are imprinted in its chemical

[★] Full Table 2 is only available at the CDS via anonymous ftp to cdsarc.cds.unistra.fr (130.79.128.5) or via <https://cdsarc.cds.unistra.fr/viz-bin/cat/J/A+A/676/A47>

composition, mass-loss, and flat stellar mass function, supporting its origin in the inner thin disc or the bulge.

NGC 6791 has one of the largest populations of BSSs among all known open clusters (Jadhav & Subramaniam 2021). The BSSs result from binary interactions such as collisions (Hills & Day 1976) or mergers (Perets & Fabrycky 2009). However, determining the formation pathway followed by this open cluster is difficult because of the incomplete parameterisation of such systems. The mass of the BSS, stellar rotation, abundance peculiarities, and characteristics of the donor remnant can be used to identify the formation pathway.

In this work, we analysed the UV-bright population of NGC 6791 using multi-wavelength spectral energy distributions (SEDs). In Sect. 2, we provide details of the data and analytical methods, and in Sect. 3 we present our results and their implications. The results are discussed in Sect. 4 and summarised in Sect. 5.

2. Data and analysis

2.1. UVIT data and Gaia membership

We observed NGC 6791 in August 2017 with the Ultraviolet Imaging Telescope (UVIT) onboard AstroSat observatory (proposal ID: A03_008). The UVIT performs observations in far-UV (FUV; 130–180 nm), near-UV (NUV; 200–300 nm), and VIS (350–550 nm) channels. More details of the calibration and instrumentation are presented in Kumar et al. (2012) and Tandon et al. (2017, 2020). The exposure times, source detections, and other observational details are given in Table 1. The UVIT data reduction and astrometry were performed using CCDLAB (Postma & Leahy 2017, 2020). The point spread function photometry of the UVIT images was carried out with IRAF (Tody 1993). Preliminary analysis and cross-matching were performed with TOPCAT (Taylor 2005).

We used the *Gaia* DR2 (Gaia Collaboration 2016, 2018)-based membership catalogue by Cantat-Gaudin et al. (2020), which is one of the most recent membership catalogues available, and the inclusion of *Gaia* DR3 data does not significantly improve the membership for the bright stars targeted in this study. The catalogue contains 1654 members with probability ≥ 0.6 . Figure 1a shows the spatial distribution of the *Gaia* members. Figure 1b shows the spatial distribution of UVIT-detected sources. The magnitude versus error distribution for UVIT filters is shown in Fig. 1c. Among the *Gaia* members, 91 are detected in at least one UV filter. The numbers of UV-detected members in individual filters are given in Table 1.

2.2. Colour–magnitude diagrams

Figure 1d shows the *Gaia* colour–magnitude diagrams (CMDs) of NGC 6791. The isochrones shown are generated using PARSEC v3.7 (Bressan et al. 2012) with $\log(\text{age}) = 9.93$, $[\text{M}/\text{H}] = 0.4$, distance modulus = 13.085 mag and $A_v = 0.302$ mag (Bossini et al. 2019). Also shown are the WD cooling curves (Bédard et al. 2020 and references therein) with a mass of $0.5 M_\odot$, which is the expected mass of WDs based on the cluster turn-off and WD initial-final mass relation (Cummings et al. 2018). Figure 1d shows that UVIT has detected stars in the MS, RGB, BSS, and hot subdwarf (sdA, sdB) phases. The sources with UV excess (see Sect. 2.3) are present on the MS and RGB. The UV-optical CMD in Fig. 1e shows the UV-detected members in the UVIT/N263M filter.

2.3. Spectral energy distributions

We visually checked the neighbourhoods ($\sim 3''$) of all 91 UV-detected sources to remove 29 sources with bright neighbours. We then constructed the SEDs of 62 isolated sources using AstroSat/UVIT, *Gaia* EDR3 (Gaia Collaboration 2021), *Swift*/UVOT (Siegel et al. 2019), Pan-STARRS (Chambers et al. 2016), 2MASS (Skrutskie et al. 2006), and WISE (Wright et al. 2010). The virtual observatory cross-matching was done using VOSA (Bayo et al. 2008) and Vizier (Ochsenbein et al. 2000). The sources were extinction corrected using known extinction–wavelength relations (Fitzpatrick 1999; Indebetouw et al. 2005).

We used VOSA¹ to fit Kurucz models (Castelli & Kurucz 2003) to the SEDs using a χ^2 minimisation technique. The metallicity of the Kurucz model was fixed to +0.5 (closest to the cluster metallicity of +0.4). Also, we fixed the distance to 4139 ± 100 pc and A_v to 0.302 ± 0.005 . The free parameters were temperature (3500–50 000 K) and $\log g$ (2–5). However, note that the SED-derived $\log g$ parameter is imprecise. After fitting the SEDs, we calculated the fractional residual as follows:

$$\text{Fractional residual} = \frac{F_{\text{obs}} - F_{\text{model}}}{F_{\text{obs}}}. \quad (1)$$

The fractional residual is shown in the bottom subpanels of the SEDs (Fig. 2).

Of the 62 isolated sources, 29 show more than 0.5 fractional residual in at least one UV filter. In the UOCS series of papers, we use Kurucz models to fit the SEDs, as they cover a wide range of wavelengths. In this study, we checked whether the detected UV excess changes are due to underestimation of the Wein tail flux in the Kurucz models. To this end, we created a hybrid Kurucz+UVBLUE model, which uses specialised UVBLUE models (Rodríguez-Merino et al. 2005) in the 850–4700 Å region and Kurucz models for the remaining red part of the spectrum. The UVBLUE models were convolved with the UVIT and UVOT filters (where the complete filter falls within UVBLUE’s range) to get synthetic photometry for a temperature range of 3000–50 000 K, $\log g$ range of 0–5, and a metallicity range of -2 to 0.5. The filter transmission profiles were taken from the SVO Filter Profile Service² (Rodrigo et al. 2012; Rodrigo & Solano 2020). We were able to fit nine stars as single stars with this hybrid model using the Python code BINARY_SED_FITTING³ (Jadhav et al. 2021). This leaves 20 sources with UV excess using the Kurucz+UVBLUE models.

The UV excess has been linked to the presence of hot compact objects such as WDs (Jadhav et al. 2019; Rao et al. 2022; Panthi et al. 2022) or hot subdwarfs (Jadhav et al. 2021). One can use double-component SED fitting to deconvolve the two stars. As VOSA cannot use hybrid models, we used BINARY_SED_FITTING to perform double-component fits using the hybrid model for the primary star (Kurucz+UVBLUE) and the Koester model (Tremblay & Bergeron 2009; Koester 2010) for the possible hotter companion (see Jadhav 2022 for more details). We were able to fit ten sources with satisfactory double components, while the remaining ten could not be fitted with available data.

The results of single- and double-component SED fitting are given in Table 2. An extended table, which includes photometry and fitting parameters, is available as supplementary material and on the CDS. Figure 2 shows the SED fits for single- and

¹ <http://svo2.cab.inta-csic.es/theory/vosa/index.php>

² <http://svo2.cab.inta-csic.es/theory/fps/>

³ https://github.com/jikrant3/Binary_SED_Fitting

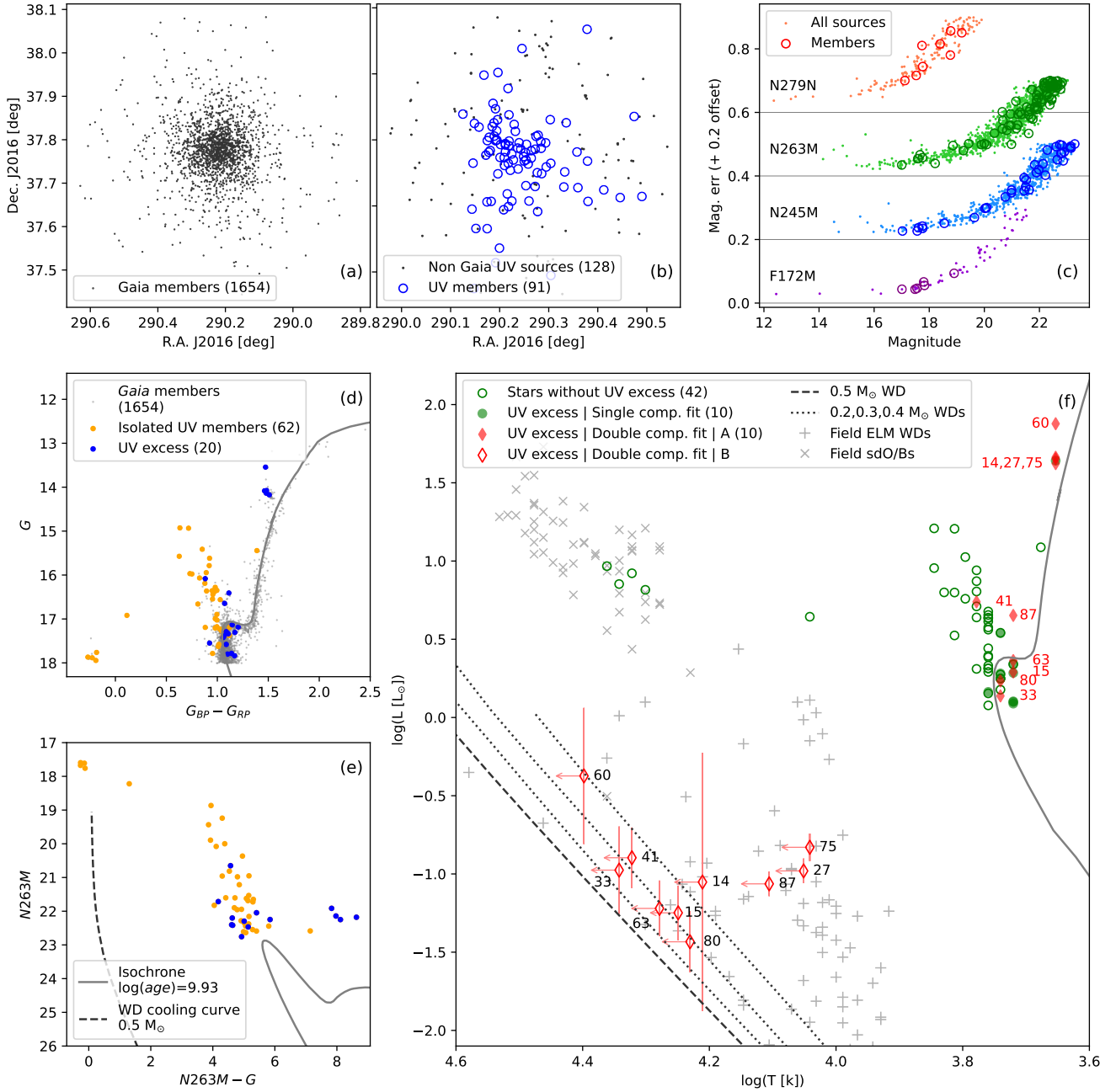


Fig. 1. Properties of UVIT photometry and HR diagrams of analysed members. (a) Spatial distribution of *Gaia* members. (b) Spatial distribution of UV-detected members (blue circles) and UV-detected sources not present in the *Gaia* EDR3 catalogue (grey dots). (c) Magnitude vs. error plots for UVIT photometry. (d) *Gaia* CMD showing the Cantat-Gaudin et al. (2020) members (as grey), UV-detected members (as orange), and members with UV excess (as blue). (e) The UV-optical CMD of cluster members. (f) The HR diagram created using SED fitting results. The figure shows 42 sources without UV excess (hollow green circles) and ten sources with UV excess (green filled circles) modelled using single-component SED. The ten sources with double-component fitting are shown as hollow red squares and red-filled squares for A and B components, respectively. Their corresponding IDs are also shown. The isochrone of $\log(\text{age}) = 9.93$ (grey curve), the $0.5 M_{\odot}$ WD cooling curve (black dashed curve), and the $0.2\text{--}0.4 M_{\odot}$ WD cooling curves (black dotted curves) are shown wherever needed in (d)–(f).

double-component fitting for the 20 sources with UV excess. The observed data points and associated error bars are shown in black. The line plots connecting estimated flux from synthetic photometry of the various models are shown in different colours (red: Kurucz+UVBLUE model, blue: Koester model, green: total flux of Kurucz+UVBLUE and Koester models). In the double SEDs, the cooler component (Kurucz or Kurucz+UVBLUE model) is denoted ‘A’, while the hotter component (Koester model) is denoted ‘B’.

In the double-component fitting, the parameters for the cooler model SED are improved as the effects of any potential hotter companion or unusual activity are reduced. However, we find that the parameter estimates derived from only 1–2 UV data points are only partially reliable. The luminosity values are relatively accurate, but the temperature may be underestimated (\equiv overestimated radius; Jadhav et al., in prep.). We therefore recommend not using the temperature or radius estimates of the hotter model SEDs.

Table 1. Exposure times in UVIT filters and detected sources.

Filter	Exp. time [s]	Detections	Members
F172M	3017.251	55	6
N245M	1259.539	734	35
N263M	1156.669	1180	81
N279N	364.296	165	8

3. Results

3.1. General comments on the SED results

Figure 1d shows that most of the BSSs are detected in NUV along with some MS stars and RGBs. We find UV excess in 20 of these sources. Among them, 12 are MS stars, 3 are BSSs, and 5 are giants. Figure 1e demonstrates the excess flux in these sources as the MS stars and RGBs are brighter than the isochrone, and moreover all the sources detected in the UV and located on the MS have some fraction of excess flux in the NUV. The remaining 42 isolated UVIT-detected stars (21 BSSs, 15 MS, 1 RGB, 4 sdBs, and 1 sdA) do not show significant UV excess.

The SED fitting gives the temperatures, luminosities, and radii of the sources. The temperature range for BSSs is 5250–7000 K while for MS stars it is 5250–6000 K. Figure 1f shows the Hertzsprung–Russell (HR) diagram of the SED fitting results. We also include the parameters of the potential hotter companions. If these latter were real, their luminosities would be of the order of $0.1 L_{\odot}$. Their SED-based temperatures are 11 000–25 000 K, and their radii are 0.02 – $0.11 R_{\odot}$. They could be (i) sub-luminous sdAs/sdBs, (ii) ELM WDs, or (iii) bloated proto-WDs (e.g., Brogaard et al. 2018), or (iv) their actual temperature could be significantly larger, which would mean these radii are overestimated, which could make them typical WDs. The grey markers in the background show the HR diagram positions of field ELMs and field sdO/sdBs for comparison. The field ELMs are a subsample of sources in Brown et al. (2016). The field sdO/sdBs are a subsample of hot subdwarfs given in Geier (2020). Both samples were fitted with single-component Kurucz SEDs using VOSA.

In the course of the SED fitting, we also tried making only Kurucz and Koester model binary SEDs. This resulted in 29 sources with UV excess, among which 10 gave satisfactory double fits. Among these latter, six were common with the hybrid and Koester fit, while four are currently classified as single fits with UV excess (star4, star19, star70 and star73). Four current binary systems (star15, star63, star80 and star87) could not be fit satisfactorily with Kurucz and Koester models using VOSA. The total number of satisfactory binary fits is the same regardless of whether or not we include UVBLUE models, and the same is true for the unsatisfactory fits. We explored whether or not there is any specific dependency, and in the case of UVBLUE models, the NUV flux for stars cooler than 6000 K is more than the Kurucz models, whereas the difference is marginal in the case of hotter stars. In general, the estimated temperatures of hotter companions were found to be higher if the UVBLUE models were incorporated. Overall, the number of sources with successful binary fits is the same in either approach; however, the overall number of sources with UV excess is reduced if UVBLUE is included.

3.2. Comments on individual systems

We did not create SEDs of UV-detected stars with neighbours within $5''$. Among them, there is a notable contact binary, V5

($P = 0.31265938$ d; Sanjayan et al. 2022a; Mochejska et al. 2003). There are also a few variables (long period, non-periodic, rotational variables): KIC 2437079 (Sanjayan et al. 2022a), V65 ($P \sim 11.3$ d), V66 ($P \sim 49$ or 99 d), and V19 (Mochejska et al. 2003). These stars are not discussed further due to them having close neighbours.

Hot subdwarfs. Star7 (B5, KIC 2437937), star49 (B4, KIC 2438324), and star79 (B3, KIC 2569576) are known pulsators (Sanjayan et al. 2022a). Star48 (B6) and star79 are RV variables and likely binary systems (Sanjayan et al. 2022b). Star49 is also an RV variable with $P = 0.398495$ d and a low-mass MS companion (Sanjayan et al. 2022b)⁴. The SED temperatures (using Kurucz models) for the three hot subdwarfs are slightly underestimated compared to Sanjayan et al. (2022b) (using Tlusty models), which is likely due to differences in the models.

Blue straggler stars. Star41 (KIC 2437238) showed rotational variability (Sanjayan et al. 2022a) and significant UV excess hinting at a $\geq 0.25 M_{\odot}$ WD as its companion. The absence of eclipses and RV variability suggests a low inclination orbit in the potential binary system. The single-lined spectroscopic binary (SB1) and γ Dor type star47 (V106, KIC 2438249, WOCS 54008) showed no excess UV flux, which is expected as Brogaard et al. (2018) derived the temperatures of binary components as $7110 + 6875$ K and their masses as $1.62 + 0.176 M_{\odot}$. The low temperatures are not enough to create significant UV flux (we note that the SED estimated radius of the BSS is overestimated as we modelled both components as a single source). The system is an eclipsing W Uma binary system with $P = 1.4464$ d (Tofflemire et al. 2014). The absence of UV excess and the low temperature of the companion suggests that significant time has passed since the mass-transfer event. The system is a prime candidate for a detailed asteroseismic study to constrain the internal structure and mass-transfer history in BSSs. Star53 (KIC 2437338) also showed rotational variability (Sanjayan et al. 2022a) but no UV excess or RV variability. Star61 showed UV excess, but we could not fit a hotter companion. Star69 (KIC 2437745) is a rapid rotator and photometric variable ($P = 1.43$) (Tofflemire et al. 2014; Sanjayan et al. 2022a). However, it did not show UV excess. Star76 (WOCS 46008, KIC 2436421) is SB1 and a rapid rotator (Tofflemire et al. 2014). Sanjayan et al. (2022a) detected variability in its *Kepler* light curves with a period of 1.44 days. However, we did not detect any UV excess and cannot not confirm whether the RV variability is periodic (with 1.44 d) due to poor sampling. Star87 shows UV flux compatible with an ELM WD. Star90 is an RV-constant star with no UV excess. Tofflemire et al. (2014) suggested that it is a $1.9 M_{\odot}$ merger product formed 1 Gyr ago in line with the absence of any hotter companion.

Red clump stars. There are 19 red clump stars identified using asteroseismic measurements (Stello et al. 2011) in NGC 6791. UVIT detected four of them, all with significant UV excess (only three are successfully fitted with a double SED). Among them, star27 (KIC 2438051), star73 (KIC 2436732), and star75 (KIC 2569055) are known pulsating red clump stars. These red clump stars did not show detectable RV variability or eclipses.

Main sequence stars. Star33 (*Gaia* DR3 2051286413614 206208) has been classified as an eclipsing binary with a period

⁴ Mochejska et al. (2003) stated $P = 0.796993$ d $\sim 2 \times 0.398495$ d.

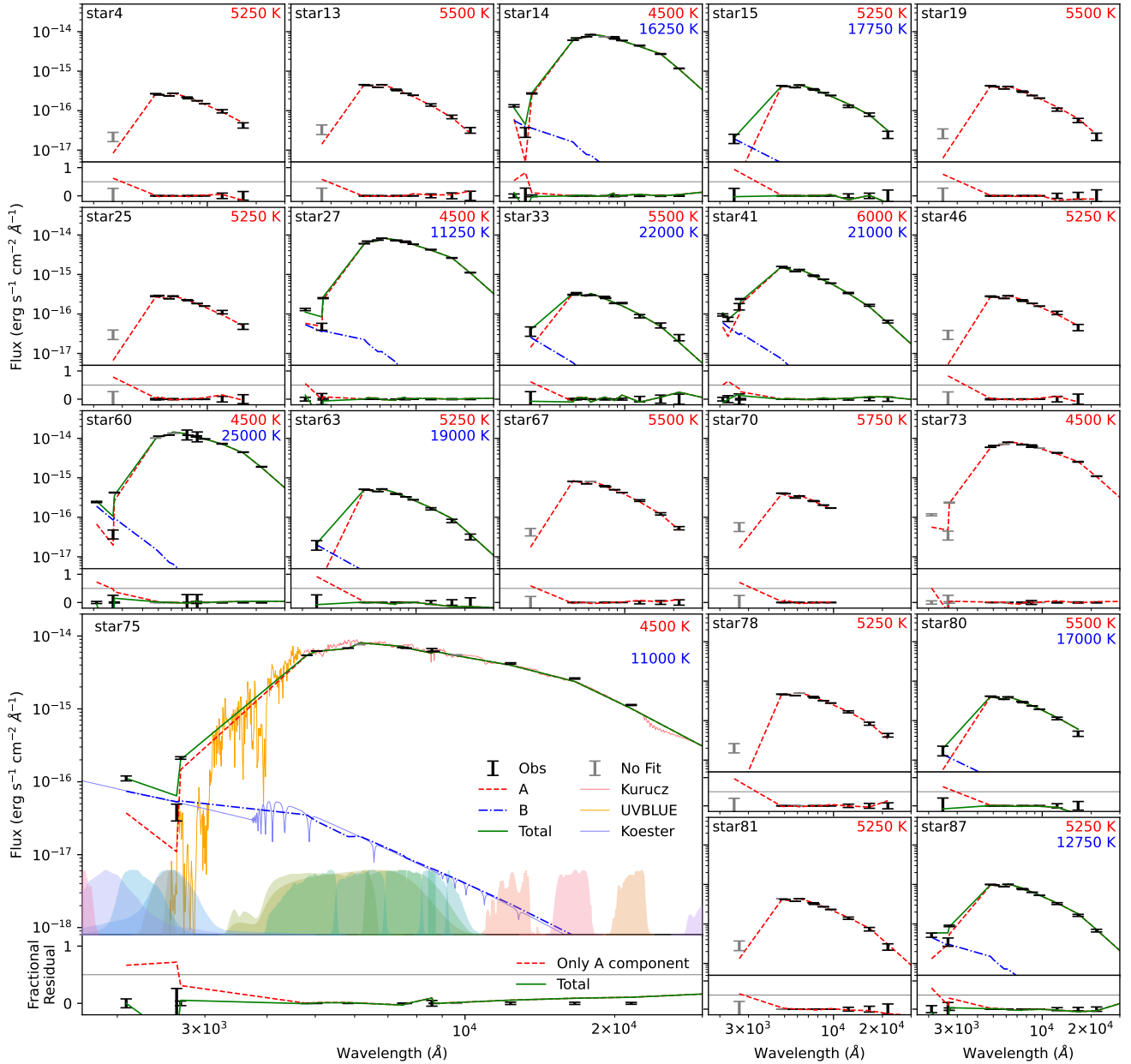


Fig. 2. SEDs of stars with fractional UV excess of more than 0.5 in at least one filter. The top panel for each star shows the observed flux (black error bars), data omitted while fitting the SED (grey error bars), the fitted Kurucz+UVBLUE model (red dashed curve), the fitted Koester model (blue dot-dashed curve; wherever applicable), and total model flux (green curve; wherever applicable). The bottom panel shows the residual flux after the single component fit (red dashed curve) and the double component fitting (green curve). The panel for star75 shows extra details such as the high-resolution spectral models (Kurucz: red, UVBLUE: orange, Koester: blue) and the used filter transmission curves (filled curves at the bottom).

of 0.3664 d (Gaia Collaboration 2022; Mowlavi et al. 2023). The *Gaia* light curves and the double-component fitting both suggest a close hotter star as its companion. However, more RV variation analysis is needed to confirm the companion and any mass-transfer history. The HR diagram positions of companions to star15, star63, and star80 indicate that they are likely WDs with mass $\gtrsim 0.3 M_{\odot}$.

Post-horizontal branch star. Star60 (WOCS 9007) is a proper-motion member of the cluster. However, its RV is different from the cluster by $\sim 25 \text{ km s}^{-1}$ with a parallax of $0.2901 \pm 0.0115 \text{ mas yr}^{-1}$ (cluster parallax is $0.241 \text{ mas yr}^{-1}$). It showed significant UV excess indicative of a young ELM companion. However, if the star is not a cluster member, then the

distance measurement and the derived classification may be incorrect.

4. Discussion

The five single hot subdwarfs detected in UV all require mass transfer for their formation (Heber 2009). None of the hot subdwarfs show UV/IR excess flux, which indicates that their subdwarf component is the dominant flux emitter in the UV–IR range. Furthermore, the hotter companion candidates in three red clumps, that is, four MS stars, two BSS, and one post-HB star, are also likely low-luminosity sdAs/sdBs or ELMs according to their HR diagram position. If these are indeed hot subdwarfs

Table 2. List of target stars along with the comments from [Tofflemire et al. \(2014\)](#), [Sanjayan et al. \(2022a\)](#) and this work.

Name	α_{J2016} [°]	δ_{J2016} [°]	Comment	Name	α_{J2016} [°]	δ_{J2016} [°]	Comment
	No UV excess			star56	290.257766	37.763117	MS
star0	290.182556	37.706893		star57	290.178641	37.803567	BSS
star1	290.330379	37.728380		star58	290.377713	37.966663	BSS
star2	290.272239	37.785515		star59	290.196283	37.748383	
star3	290.278053	37.806657		star61	290.273850	37.804970	
star5	290.180772	37.783681		star62	290.302801	37.830190	BSS
star6	290.143487	37.695005		star64	290.411506	37.724085	MS
star7	290.263954	37.783218	sdB, Puls	star65	290.217391	37.764303	
star8	290.174187	37.706013	MS	star66	290.215274	37.718092	BSS
star9	290.229360	37.822990		star68	290.211291	37.792004	
star10	290.167968	37.897422	sdA	star69	290.248584	37.774346	BSS, RR, Variable
star11	290.237421	37.755679	BSS	star71	290.186347	37.854764	MS
star12	290.332132	37.751261	MS	star72	290.303946	37.594908	MS
star16	290.200673	37.773090		star74	290.209131	37.772973	BSS
star17	290.293412	37.795104	BSS, SB1, RR	star76	290.145732	37.764532	BSS, SB1, RR, Variable
star18	290.191630	37.798388		star77	290.147393	37.575227	BSS
star20	290.217878	37.698901	MS	star79	290.188213	37.825343	sdB, Puls
star21	290.242940	37.785566	BSS, SB1	star82	290.231777	37.812650	
star22	290.224330	37.778367		star83	290.264080	37.772164	
star23	290.254358	37.792965		star84	290.253508	37.769471	BSS
star24	290.191568	37.614156	BSS	star85	290.357116	37.781353	MS
star26	290.259442	37.707294	MS	star86	290.253143	37.730550	
star28	290.245497	37.937647	BSS	star88	290.358896	37.727381	MS
star29	290.201645	37.792628		star89	290.211412	37.793906	
star30	290.194181	37.799349	BSS	star90	290.249771	37.767570	BSS
star31	290.221496	37.753805		UV excess – Single fit			
star32	290.284253	37.786966		star4	290.196492	37.901509	MS
star34	290.236587	37.787253	MS	star13	290.239528	37.795310	MS
star35	290.199415	37.636157	MS	star19	290.195735	37.830140	MS
star36	290.216948	37.877327		star25	290.184428	37.819743	MS
star37	290.276987	37.691396		star46	290.378518	37.767541	MS
star38	290.473241	37.834930	MS	star67	290.252538	37.780422	BSS
star39	290.193870	37.813223		star70	290.271927	37.729174	MS
star40	290.209807	37.760943	BSS	star73	290.174902	37.798373	RC
star42	290.224628	37.707220	BSS, SB1	star78	290.148421	37.824601	MS
star43	290.218488	37.790879		star81	290.444898	37.712358	MS
star44	290.207915	37.694110		UV excess – Double fit			
star45	290.379465	37.706632	MS	star14	290.218634	37.837626	RC
star47	290.294602	37.758718	BSS, γ Dor Puls	star15	290.157917	37.819014	MS
star48	290.188867	37.805342	sdB	star27	290.276235	37.749896	RC
star49	290.303713	37.764194	sdB, Puls	star33	290.151458	37.665758	MS, ECL
star50	290.191585	37.846677	RGB	star41	290.211737	37.781781	BSS, Rot. var.
star51	290.285072	37.748605		star60	290.283629	37.797057	post-HB
star52	290.174360	37.665663	MS	star63	290.335191	37.825374	MS
star53	290.218961	37.797860	BSS, Rot. var.	star75	290.125237	37.838649	RC
star54	290.489114	37.714080		star80	290.171933	37.776700	MS
star55	290.177668	37.781130	BSS, RR	star87	290.227669	37.769334	BSS

Notes. BSS: blue straggler star, ECL: eclipsing binary, HB: horizontal branch, Puls: pulsator, RC: red clump, Rot. var: rotational variable, RR: rapid rotator. An extended table with UVIT photometry for all 91 UV-detected members and SED fitting parameters of the 62 isolated sources of our sample is given as supplementary material and available at the CDS.

or ELMs, then it means that all these are post-mass-transfer systems. Among the double SED-fitted MS stars, star33 is a known binary with a close companion. The MS stars that have accreted mass are known as blue lurkers ([Leiner et al. 2019](#); [Jadhav 2022](#)). These are the MS equivalents of the BSSs. As such, they would be similar to BSSs in terms of formation scenarios (mergers or mass transfer) and detection techniques

(high rotation, chemical peculiarities, post-mass-transfer companions). Star33 is therefore a prime candidate for being a blue lurker. At the same time, the other three MS stars are also blue lurker candidates subject to confirmation of the nature of the companion. If confirmed, this will make NGC 6791 one of the few clusters known to host blue lurkers. However, further observational evidence of rapid rotation and chemical alteration is

necessary to confirm their status as blue lurkers. We note that this cluster has several short-period binaries, suggestive of possible Case-A/Case-B-mode mass transfer, which can lead to binaries with very low-mass stellar remnants (e.g., star47). The UV images are able to detect hotter systems, and there could be many more that are beyond the detection limit of UVIT. We note that such systems are found across the evolutionary stages from MS to post-HB.

The only detected RGB star shows UV excess when fitted with Kurucz models, which could later be explained by the updated Wein tail of UVBLUE models. The other five giants (four red clumps and one post-HB) show significant UV excess flux. NUV excess in RGBs has been known to be caused by rotation (Dixon et al. 2020). However, a hot compact companion can also give rise to UV excess. UV spectroscopy is required to confirm the exact source of the NUV flux from these RGBs.

Given the distance of NGC 6791, only the brightest WDs will be visible even in UV (all single subdwarfs detected presently are brighter than $\approx 6 L_{\odot}$). After cross-matching with the *Hubble* Space Telescope proper motion catalogue of NGC 6791 (Libralato et al. 2022), we were able to identify one WD candidate (290.20235, 37.76336 at 21.83 mag in F814W) within the small footprint covered by the *Hubble*. However, there are insufficient data points to parameterise it using its SED. There could be more such member WDs present, which could be discovered after deep multi-epoch wide-field imaging, such as that carried out by the Legacy Survey of Space and Time (Ivezić et al. 2019).

The colour of BSSs in the CMD has been linked with their origin. Ferraro et al. (2009) claimed that bluer BSSs in the globular cluster M 30 are formed via collisional mergers, while redder BSSs are formed via mass transfer. Similar double BSS sequences have been seen in other globular clusters (NGC 362: Dalessandro et al. 2013; Dattatreya et al. 2023, NGC 2173: Li et al. 2018). Similarly, the UV excess of BSSs has been linked to binarity (Gosnell et al. 2015; Sindhu et al. 2019; Pandey et al. 2021). In NGC 6791, the three BSSs with UV excess (indication of binarity) are generally redder than the rest of the BSSs of similar luminosity. This could be similar to the colour-dependent formation scenarios proposed by Ferraro et al. (2009). However, a bigger sample is needed to reach a statistically significant conclusion.

NGC 6791 has single sdBs and one sdA, along with possible low-luminosity sdBs and ELMs as companions to stars in different evolutionary phases. All of these factors suggest that the binaries play a very significant role in this dynamically old system, resulting in the formation of various types of stars due to differences in the masses of the binary members as well as their orbital properties. Therefore, this old open cluster is unique in possessing several features arising out of dynamics and binary systems.

5. Summary and conclusion

UVIT detected 91 members of NGC 6791 in either FUV or NUV filters, including MS, BSSs, hot subdwarfs, RGBs, and red clump stars. We provide SED-based parameters for 62 of the isolated sources. Of these sources, 20 showed UV excess flux, which is an indicator of a hot compact binary companion. We estimated approximate parameters for ten potential compact binary companions using SED analysis.

The total number of satisfactory binary fits is the same if we use a hybrid of UVBLUE+Kurucz models, but the number of sources with UV excess is higher without UVBLUE. In general,

we estimated higher temperatures for hotter companions when the UVBLUE models were included.

NGC 6791 contains a significant population of single hot subdwarfs (four sdB and one sdA) and optically subluminescent compact objects (ten hot subdwarf/ELMs). This is unique in open clusters and likely due to the dense and rich nature of NGC 6791. There are four blue lurker candidates in the cluster, which need to be confirmed using a combination of abundance studies, UV spectroscopy, rotational velocity, and RV/flux time series analysis. We note the presence of candidate post-mass-transfer systems across the evolutionary phases in this cluster, from MS to RGB, HB, and post-HB, suggestive of a rich population of interacting binaries.

The cluster appears to show properties similar to those of low-density globular clusters, along with some features seen in open clusters. This cluster is therefore a potential test bed, ideal for performing numerical simulations in order to understand the underlying processes regarding dynamics, binarity, and stellar evolution.

Acknowledgements. We thank the anonymous referee for constructive comments, which helped improve the methodology and discussion. VJ thanks the Alexander von Humboldt Foundation for their support. AS thanks for the support of the SERB power fellowship. RS thanks the National Academy of Sciences, India (NASI), Prayagraj, for the award of a NASI honorary Scientist position; the Alexander von Humboldt Foundation, Germany, for the award of Group linkage long-term research program between IIA, Bengaluru and European Southern Observatory, Munich, Germany, and the Director, IIA for providing institutional, infrastructural support during this work. UVIT project is a result of the collaboration between IIA, Bengaluru, IUCAA, Pune, TIFR, Mumbai, several centres of ISRO, and CSA. This publication uses VOSA, developed under the Spanish Virtual Observatory project.

References

- Bayo, A., Rodrigo, C., Barrado Y Navascués, D., et al. 2008, *A&A*, 492, 277
 Bédard, A., Bergeron, P., Brassard, P., & Fontaine, G. 2020, *ApJ*, 901, 93
 Bossini, D., Vallenari, A., Bragaglia, A., et al. 2019, *A&A*, 623, A108
 Bressan, A., Marigo, P., Girardi, L., et al. 2012, *MNRAS*, 427, 127
 Brogaard, K., Christiansen, S. M., Grundahl, F., et al. 2018, *MNRAS*, 481, 5062
 Brown, W. R., Gianninas, A., Kilic, M., Kenyon, S. J., & Allende Prieto, C. 2016, *ApJ*, 818, 155
 Cantat-Gaudin, T., Anders, F., Castro-Ginard, A., et al. 2020, *A&A*, 640, A1
 Castelli, F., & Kurucz, R. L. 2003, *New Grids of ATLAS9 Model Atmospheres*, eds. N. Piskunov, W. W. Weiss, & D. F. Gray, IAU, ASP, A20
 Chambers, K. C., Magnier, E. A., Metcalfe, N., et al. 2016, arXiv e-prints [arXiv:1612.05560]
 Cummings, J. D., Kalirai, J. S., Tremblay, P. E., Ramirez-Ruiz, E., & Choi, J. 2018, *ApJ*, 866, 21
 Dalessandro, E., Ferraro, F. R., Massari, D., et al. 2013, *ApJ*, 778, 135
 Dattatreya, A. K., Yadav, R. K. S., Rani, S., et al. 2023, *ApJ*, 943, 130
 Dixon, D., Tayar, J., & Stassun, K. G. 2020, *AJ*, 160, 12
 Ferraro, F. R., Beccari, G., Dalessandro, E., et al. 2009, *Nature*, 462, 1028
 Fitzpatrick, E. L. 1999, *PASP*, 111, 63
 Gaia Collaboration (Prusti, T., et al.) 2016, *A&A*, 595, A1
 Gaia Collaboration (Brown, A. G. A., et al.) 2018, *A&A*, 616, A1
 Gaia Collaboration (Brown, A. G. A., et al.) 2021, *A&A*, 649, A1
 Gaia Collaboration (Vallenari, A., et al.) 2022, *A&A*, 674, A1
 Geier, S. 2020, *A&A*, 635, A193
 Gosnell, N. M., Mathieu, R. D., Geller, A. M., et al. 2015, *ApJ*, 814, 163
 Heber, U. 2009, *ARA&A*, 47, 211
 Hills, J. G., & Day, C. A. 1976, *Astrophys. Lett.*, 17, 87
 Indebetouw, R., Mathis, J. S., Babler, B. L., et al. 2005, *ApJ*, 619, 931
 Ivezić, Ž., Kahn, S. M., Tyson, J. A., et al. 2019, *ApJ*, 873, 111
 Jadhav, V. V. 2022, PhD thesis, IISc, India
 Jadhav, V. V., & Subramaniam, A. 2021, *MNRAS*, 507, 1699
 Jadhav, V. V., Sindhu, N., & Subramaniam, A. 2019, *ApJ*, 886, 13
 Jadhav, V. V., Pandey, S., Subramaniam, A., & Sagar, R. 2021, *J. Astrophys. Astron.*, 42, 89
 Kamann, S., Bastian, N. J., Gieles, M., Balbinot, E., & Hénault-Brunet, V. 2019, *MNRAS*, 483, 2197
 Koester, D. 2010, *Mem. Soc. Astron. Ital.*, 81, 921

- Kumar, A., Ghosh, S. K., Hutchings, J., et al. 2012, [Ultra Violet Imaging Telescope \(UVIT\) on ASTROSAT, Proc. SPIE](#), 8443, 84431N
- Leiner, E., Mathieu, R. D., Vanderburg, A., Gosnell, N. M., & Smith, J. C. 2019, [ApJ](#), 881, 47
- Li, C., Deng, L., de Grijs, R., Jiang, D., & Xin, Y. 2018, [ApJ](#), 856, 25
- Libralato, M., Bellini, A., Vesperini, E., et al. 2022, [ApJ](#), 934, 150
- Martinez-Medina, L. A., Gieles, M., Pichardo, B., & Peimbert, A. 2018, [MNRAS](#), 474, 32
- Mochejska, B. J., Stanek, K. Z., & Kaluzny, J. 2003, [AJ](#), 125, 3175
- Mowlavi, N., Holl, B., Lecoœur-Taïbi, I., et al. 2023, [A&A](#), 674, A16
- Ochsenbein, F., Bauer, P., & Marcout, J. 2000, [A&AS](#), 143, 23
- Pandey, S., Subramaniam, A., & Jadhav, V. V. 2021, [MNRAS](#), 507, 2373
- Panthi, A., Vaidya, K., Jadhav, V., et al. 2022, [MNRAS](#), 516, 5318
- Perets, H. B., & Fabrycky, D. C. 2009, [ApJ](#), 697, 1048
- Postma, J. E., & Leahy, D. 2017, [PASP](#), 129, 115002
- Postma, J. E., & Leahy, D. 2020, [PASP](#), 132, 054503
- Rao, K. K., Vaidya, K., Agarwal, M., et al. 2022, [MNRAS](#), 516, 2444
- Rodrigo, C., & Solano, E. 2020, [XIV.0 Scientific Meeting\(virtual\) of the Spanish Astronomical Society](#), 182
- Rodrigo, C., Solano, E., & Bayo, A. 2012, [SVO Filter Profile Service Version 1.0, IVOA Working Draft 15 October 2012](#)
- Rodríguez-Merino, L. H., Chavez, M., Bertone, E., & Buzzoni, A. 2005, [ApJ](#), 626, 411
- Sahu, S., Subramaniam, A., Simunovic, M., et al. 2019, [ApJ](#), 876, 34
- Sanjayan, S., Baran, A. S., Németh, P., et al. 2022a, [Acta Astron.](#), 72, 77
- Sanjayan, S., Baran, A. S., Ostrowski, J., et al. 2022b, [MNRAS](#), 509, 763
- Siegel, M. H., LaPorte, S. J., Porterfield, B. L., Hagen, L. M. Z., & Gronwall, C. A. 2019, [AJ](#), 158, 35
- Sindhu, N., Subramaniam, A., Jadhav, V. V., et al. 2019, [ApJ](#), 882, 43
- Skrutskie, M. F., Cutri, R. M., Stiening, R., et al. 2006, [AJ](#), 131, 1163
- Stello, D., Meibom, S., Gilliland, R. L., et al. 2011, [ApJ](#), 739, 13
- Subramaniam, A., Pandey, S., Jadhav, V. V., & Sahu, S. 2020, [J. Astrophys. Astron.](#), 41, 45
- Tandon, S. N., Subramaniam, A., Girish, V., et al. 2017, [AJ](#), 154, 128
- Tandon, S. N., Postma, J., Joseph, P., et al. 2020, [AJ](#), 159, 158
- Taylor, M. B. 2005, in [Astronomical Data Analysis Software and Systems XIV](#), eds. P. Shopbell, M. Britton, & R. Ebert, [ASP Conf. Ser.](#), 347, 29
- Tody, D. 1993, in [Astronomical Data Analysis Software and Systems II](#), eds. R. J. Hanisch, R. J. V. Brissenden, & J. Barnes, [ASP Conf. Ser.](#), 52, 173
- Tofflemire, B. M., Gosnell, N. M., Mathieu, R. D., & Platais, I. 2014, [AJ](#), 148, 61
- Tremblay, P. E., & Bergeron, P. 2009, [ApJ](#), 696, 1755
- Vaidya, K., Panthi, A., Agarwal, M., et al. 2022, [MNRAS](#), 511, 2274
- Vernekar, N., Subramaniam, A., Jadhav, V. V., & Bowman, D. M. 2023, [MNRAS](#), 524, 1360
- Villanova, S., Carraro, G., Geisler, D., Monaco, L., & Assmann, P. 2018, [ApJ](#), 867, 34
- Wright, E. L., Eisenhardt, P. R. M., Mainzer, A. K., et al. 2010, [AJ](#), 140, 1868